Available online at www.sciencedirect.com
SCIENCE DIRECT®
Journal of Nuclear Materials 334 (2004) 71–78
journal of nuclear materials
www.elsevier.com/locate/jnucmat

Correlation between irradiation-induced changes of microstructural parameters and mechanical properties of RPV steels

J. Böhmert, H.-W. Viehrig, A. Ulbricht *

Forschungszentrum Rossendorf e.V., Institut für Sicherheitsforschung, P.O. Box 510119, D-01314 Dresden, Germany

Received 11 November 2003; accepted 28 April 2004

Abstract

Radiation hardening, displayed by the yield stress increase, and irradiation embrittlement, described by the Charpy transition temperature shift, were experimentally determined for a broad variety of irradiation specimens machined from different reactor pressure vessel base and weld materials and irradiated in several VVER-type reactors. Additionally, the same specimens were investigated by small angle neutron scattering. The analysis of the neutron scattering data suggests the presence of nano-scaled irradiation defects. The volume fraction of these defects depends on the neutron fluence and the material. Both irradiation hardening and irradiation embrittlement correlate linearly with the square root of the defect volume fraction. However, a generally valid proportionality is only a rough approximation. In detail, chemical composition and technological pretreatment clearly affect the correlation.

1. Introduction

The impact of the neutron irradiation on the mechanical properties of low alloy ferritic steels used for reactor pressure vessels (RPV) is a well-researched phenomenon. Currently, special attention is being paid to the microstructural irradiation effects for a better understanding of the underlying mechanisms. Within this frame small angle neutron scattering (SANS) has been proved to be one of the most appropriate methods to detect and to characterize the nano-scaled features produced by neutron irradiation. It can especially provide data on the size distribution of irradiation-induced microstructural defects (precipitates, clusters).

Forschungszentrum Rossendorf has extensively studied the irradiation effect on the microstructure of a broad variety of RPV materials using SANS techniques. Concurrently, the same materials have been well characterized by mechanical testing. In this way a sizable collection of data was obtained. It is the focus of this study to correlate the data characterizing neutron hardening and embrittlement with the irradiation-induced changes of the microstructure.

2. Experimental background

The material base of the investigation is a broad variation of irradiation specimens taken from the irradiation programme Rheinsberg I and II, surveillance programmes of Russian, Ukranian and Hungarian NPPs and special irradiation experiments in VVER reactors. It comprises both base metal and weld metal, steels according to manufacturer's specification, outside the specification or model alloys, VVER-type steels and ASTM-related types. Fabrication procedures, heat treatment and chemical composition varied within a broad range. The materials investigated are listed in Table 1. More details are given in [1].

* Corresponding author. Tel.: +49-351 260 3155/3154; fax: +49-351 260 2205.
E-mail address: a.ulbricht@fz-rossendorf.de (A. Ulbricht).

0022-3115/$ - see front matter © 2004 Elsevier B.V. All rights reserved.
doi:10.1016/j.jnucmat.2004.05.003

Table 1
Investigated materials

Type		Designation	Heat/code	Producer/supplier	Comment
1.1 Irradiation programme Rheinsberg I					
VVER-440	BM	15Kh2MFA	R1	Prometey RRC-KI	Russian fabrication line
			R2		
			R3		
			D25		
VVER-1000	BM	15Kh2NMFAA	R16	VNIIAES	Novovoronesh NPP, unit 5
			R17		South Ukrainian NPP, unit 1
VVER-1000	W	10KhGMFAA	R19	VNIIAES	South Ukrainian NPP, unit 1
1.2 Irradiation programme Rheinsberg II					
VVER-440	BM	15Kh2MFA	KAB-B	Greifswald	Prototype RPV steel for VVER-440/
VVER-440	W	Sv10KhMFT(u)	KAB-W	NPP	230 test heats
VVER-440	BM	15Kh2MFA	ESW-A	ESW	
			ESW-B		
			ESW-C		
			ESW-D		
ASTM-steel	BM	A533B cl. 1	JRQ	Kawasaki steel	IAEA reference material
	W		JWQ	corp.	
		A508 cl. 3	JFL		IAEA-CRP-programme
2. Surveillance programme					
VVER-440	BM	15Kh2MFAA	PA1-B	Skoda	NPP Paks, unit 1
	W	Sv10KhMFT	PA1-W		NPP Paks, unit 1
	BM	15Kh2MFA	RO-B	RRC KI	NPP Rovno, unit 1
			KO-B		NPP Kola, unit 3
VVER-440	W	Sv10KhMFT	RO-W	RRC KI	NPP Rovno, unit 1
			AR-W		NPP Armenia, unit 3
3. Model alloys					
Fe base alloy			ML-A	RRC-KI	Variation of content of P, Cu and Ni
(FeMnSi)			ML-B		
			ML-C		
			ML-D		
			ML-F		
			ML-G		
			ML-H		
4. Special irradiation					
VVER-1000	W	10KhGMFAA	TA-1	RRC-KI	Novovoronesh NPP, unit 5,
			TA-2		surveillance position

BM – base metal; W – weld metal.

Irradiations were performed at temperatures of 255 to 290 °C and neutron fluxes of 2 to 54×10^{11} n/cm^2 s [$E > 0.5$ MeV], the neutron exposure reached values between 2.6 and 630×10^{18} n/cm^2 [$E > 0.5$ MeV].

The mechanical test programme included HV10 hardness measurements, tensile tests, Charpy V-notch impact tests and fracture mechanics three-point bend tests for the T_0 determination. They were conducted in the hot cells of the Institute of Safety Research of FZR and the RRC Kurchatov Institute Moscow, respectively.

3. Microstructural analysis with SANS

SANS provides information on microstructural inhomogeneities in the size range of 1 to 500 nm and averaged over a volume of $\gg 1$ mm^2. Thus, it is especially convenient for such a correlative consideration as here presented. On the other hand, SANS is an indirect method which does not provide a real space image but only the Fourier transform of the averaged spatial scattering density distribution. From that, the real microstructure cannot be reconstructed. However, some microstructural parameters can be extracted from the scattering intensity distribution, at least by assuming a simplified structural model and by assuring suitable measuring conditions. For the analyses of this paper, the following conditions and assumptions were selected:

- The SANS intensity is measured over a large range of the scattering vector.

- A saturating magnetic field is applied during the experiment in order to separate the nuclear and magnetic contribution of the SANS intensity.
- The device-caused and incoherent scattering effects are carefully eliminated.
- The structural model is based on the two-phase approach: isolated scattering particles of low concentration in a homogeneous matrix.
- The particles are spherical, polydisperse and non-ferromagnetic.
- The particle-size distribution function is computed by the indirect transformation method developed by Glatter [2].

Under these circumstances the microstructure is characterized by

- the size distribution function of the radiation defects related to the volume fraction and the number density and given in relative units from the total, and the nuclear scattering cross section and in absolute units from the magnetic scattering cross section,
- the volume fraction c_v and the total number density N_R of microstructural defects within a selected size range,
- the defect radius at the maximum of the size distribution (mode),
- the A-ratio as ratio between total scattering cross section and nuclear scattering cross section.

The last parameter includes information about the composition and structure of the defects. The evaluation procedure is described in more detail in [3–5].

SANS measurements were conducted at different European SANS facilities using 10 mm × 10 mm × 0.8 mm slices cut from the halves of broken Charpy specimens. For the different instruments nearly the same experimental conditions were chosen. The SANS facilities used and the measuring parameters are summarized in Table 2.

4. Results

The qualitative course of the size distribution of the fine scattering heterogeneities is similar for all materials investigated. The distribution is bimodal with a steep peak near 1 nm and a broad second relative maximum of low height between 8 and 16 nm. The first peak appears in the irradiated condition and is partly or almost completely removed by annealing. Material composition and irradiation conditions do not change the position and shape but clearly affect the height of the peak. Only the very highly irradiated surveillance specimens (KO-B, AR-W) exhibit a broader first peak. The low second peak is hardly influenced by irradiation. Fig. 1 shows the volume-fraction related size distribution function for the material KAB-B as an example. The volume fraction distribution function dc_v/dR is calculated from the magnetic cross section under the above-mentioned assumption that the scattering defects are magnetic holes.

The result emphasizes that the first peak characterizes the irradiation-induced defects. The integration of the volume fraction distribution function in the range of

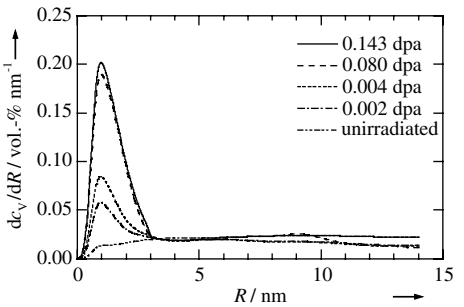

Fig. 1. Size distribution function (related to the volume fraction) dc_v/dR versus radius R of the scattering defects, obtained from SANS measurements at the 15Xh2MFA VVER 440-type RDB steel, heat KAB-B.

Table 2
SANS instruments used and measuring parameters

Instrument	SANS-V4	PAXE	D11	KWS-II	Yellow Submarine
Site	HMI Berlin (BER II)	LLB Saclay (Orphee RR)	ILL Grenoble (HFR)	FZ Jülich (DIDO)	KFKI Budapest
Beam size/mm	7.5	7.5	7.5	8.0	8.0
Wavelength/mm	0.5/0.6	0.5/0.6	0.5	0.715	0.47
Distance probe detector/m	1.086; 4.0	1.5; 5.0	1.1; 4.0; 16.5	1.5; 4.1	5.5
Q-range/nm^{-1}	0.2–3.2	0.2–2.6	0.2–4.0	0.12–1.25	0.2–0.8
Detector type	2d Position-sensitive He detector, 64 cm × 64 cm				
Magnetic field/T	1.3	1.4	1.5	1.5	<1.0
Calibration standard	Water	–	Water	Polyethylene	–

the first peak ($0 \leqslant R \leqslant 3$ nm) provides the volume fraction c_v of the ultra-fine heterogeneities for the irradiated condition and the unirradiated initial state and, eventually, their subtraction the volume fraction Δc_v of the irradiation-induced defects. Because the changes of the mode values of the defect radius are marginal, the parameter 'volume fraction' is selected as correlation parameter. Typical variations of the A-ratio with the chemical composition point to the fact that the type of the defect can also be modified.

The correlations between the irradiation-induced increase of the yield stress $\Delta R_{p0.2}$ and the shift of the Charpy transition temperature ΔTT, respectively, and the volume fraction Δc_v of the irradiation defects are depicted in Figs. 2 and 3.

The measured points represent different types of RPV steels, manufacturers, irradiation temperatures, neutron fluxes and neutron fluences. From this point of view the broad scattering range is not surprising. However, the data trend is clear: Provided that the results of the model alloys are excluded, yield stress and transition temperature increase with increasing volume fraction of the defects. Additionally, linear and square root fit lines are drawn in Figs. 2 and 3. The square-root function describes the trend better. The correlation of hardness and volume fraction shows a similar course.

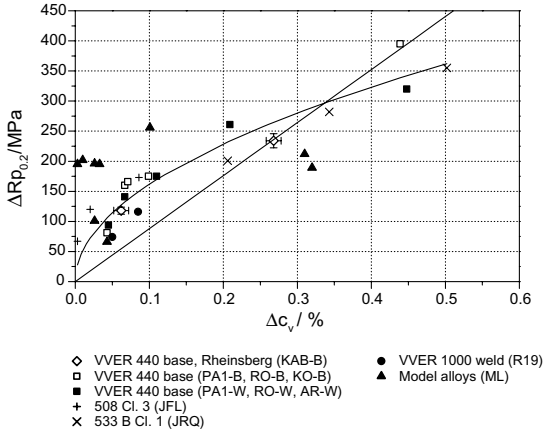

Fig. 2. Correlation between the irradiation-caused increase of the yield stress $\Delta R_{p0.2}$ and the volume fraction of the radiation defects Δc_v.

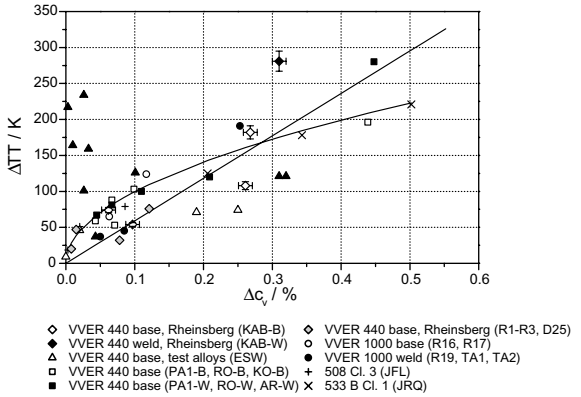

Fig. 3. Correlation between the irradiation-caused shift of the transition temperature ΔTT and the volume fraction of the irradiation defects Δc_v (ΔTT is related to a Charpy energy of 48 J).

5. Discussion

In the bainitic RPV steels, irradiation produces nano-scaled microstructural defects that are causally connected with the irradiation-induced increase of the strength and the shift of the transition temperature. The relation is especially evident if the scope of the parameters of influence is reduced. As an example, Fig. 4 illustrates the variation of the hardness HV10 with the volume fraction of nano-scaled structure defects, shown for the 10KhGMFAA VVER 1000-type weld metal (code R19) in the un- and irradiated state and after annealing at different temperatures. Although there is some scatter, the (nonlinear) correlation between both parameters is clearly demonstrated.

The reduction of the radiation defects due to thermal annealing at temperatures above the irradiation temperature decreases the hardness in the same manner as shown in Fig. 5. This shows that the activation energy is equal and proves the causal connection between both parameters.

Obviously, the fine-scale irradiation defects act as dispersed obstacles to dislocation motion. Though the type of the defects and their efficiency as obstacles for the glide dislocations have not yet fully been recognized,

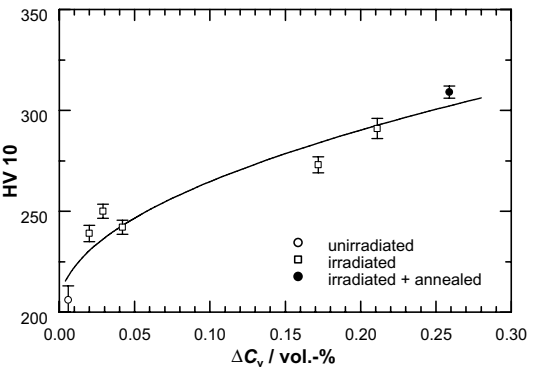

Fig. 4. Vickers hardness HV10 versus volume fraction Δc_v of nano-scaled scattering defects for the 10KhGMFAA VVER 1000-type weld metal, (heat R19) in the unirradiated and irradiated state and after annealing at different temperatures in the range of 350 to 475 °C.

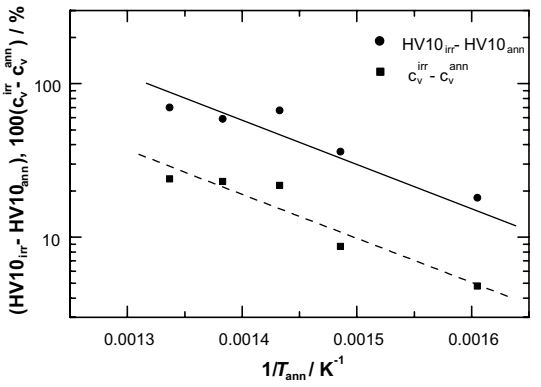

Fig. 5. Change of the Vickers hardness HV10 and of the volume fraction c_v of the irradiated state due to annealing versus the reciprocal annealing temperature T_{ann} (Arrhenius plot).

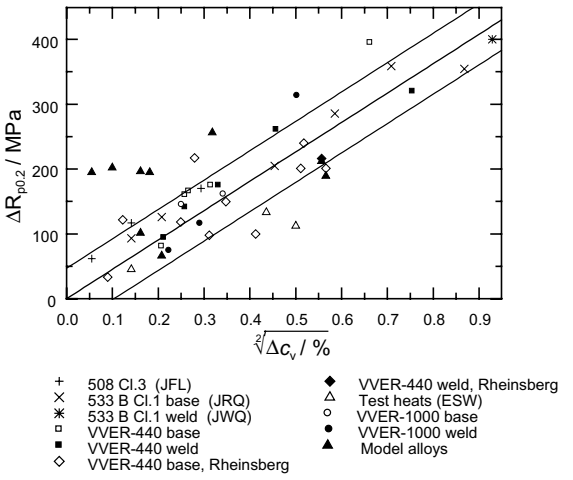

Fig. 6. Correlation between the irradiation hardening $\Delta R_{p0.2}$ and the square root of the volume fraction Δc_v of the irradiation defects.

the fine-dispersed radiation defects can be regarded as weak, penetrable obstacles. In this case, there are different theoretical approaches to the dislocation defect interaction mechanism, e.g. the Fleischer–Friedel point-obstacles approximation [6], the modulus-mismatch strengthening according to Russell and Brown [7] or the Schwarz–Labusch theory [8]. The approaches provide a proportionality to $\sqrt{\Delta c_v}$, at least for defects of constant size, of low extent and/or as a first approximation. Thus, a correlation between yield stress increase and square root of the volume fraction of the radiation defects should be expected.

Fig. 6 shows the correlation evaluated in this way. Some $R_{p0.2}$ values which were not experimentally measured are estimated from the hardness values by means of the statistically well-proved correlation obtained from the results of this working programme

$$R_{p0.2}/\mathrm{MPa} = (3.043\ \mathrm{HV10} - 114.56) \pm 40.46. \quad (1)$$

The straight lines in Fig. 6, which represent the mean values and the standard deviation, are based on the expression

$$\Delta R_{p0.2}/\mathrm{MPa} = 453\sqrt{\Delta c_v/\%} \pm 47. \quad (2)$$

They were obtained by regression fitting of all experimental results excluding the model alloys. The correlation coefficient R amounts 0.885.

Apart from the model alloys, the results of some VVER-type base metals (especially the ESW test or the surface layer of KAB) and weld (R19) as well as the highly irradiated VVER 440 surveillance metal KO-B are significantly outside the $\pm 1\sigma$ band of the fit. For the KO-B material, the SANS experiments yield a clearly higher mean size of the defects. Thus, the above-mentioned condition of the approximation (similar mode value of the size distribution function) is not fulfilled.

The consideration so far assumes a linear superposition of the hardening effects in the initial state and after irradiation. In reality the strengthening process is highly complex and different sources of strengthening combine to produce the total flow stress σ_y $(= R_{p0.2})$ [9]

$$\sigma_y = \sigma_0 + \Delta\sigma_{ss} + \Delta\sigma_{disl} + \Delta\sigma_{gr} + \Delta\sigma_{part}. \quad (3)$$

The quantity σ_0 is the temperature and strain rate sensitive frictional stress from the inherent lattice resistance to slip, $\Delta\sigma_{ss}$ is the solid solution hardening effect increasing with the content of solved foreign atoms, $\Delta\sigma_{disl}$ represents the effect due to the long range stress fields of the dislocations and is proportional to the square root of the dislocation density, $\Delta\sigma_{gr}$ is the well-known Hall–Petch grain strengthening, and $\Delta\sigma_{part}$ is the contribution of particles, precipitates or similar structural defects. The last one mainly results from the carbide dispersion in the initial state. The irradiation does not (or hardly) change the inherent lattice resistance, the grain size, the dislocation density and the carbide dispersion. It preferentially produces a new dispersion of dislocation obstacles of another (lower) efficiency and reduces the solid solution hardening term as the foreign atoms are precipitated in the radiation defects, e.g. in copper rich precipitates.

Thus, the radiation hardening, as represented by the yield stress increase $\Delta R_{p0.2}$, is described by

$$\begin{aligned}\Delta R_{p0.2} &= R^{irr}_{p0.2} - R^{un}_{p0.2} \\ &= \Delta\sigma^{irr}_{ss} - \Delta\sigma^{un}_{ss} + \Delta\sigma^{irr}_{part} - \Delta\sigma^{un}_{part}. \end{aligned} \quad (4)$$

The notations 'irr' and 'un' mean the irradiated and unirradiated states, respectively. The particle strengthening of the irradiated state $\Delta\sigma^{irr}_{part}$ results from a mixture of (at least) two different particle dispersions: the

primary particles of the as-received state ($= \Delta\sigma_{\text{part}}^{\text{un}}$) and the radiation defects. Only the last one provides the strengthening contribution $\Delta\sigma_{\text{rad}}$ which can be correlated with the volume fraction of the radiation defects. The strengthening of the particle mixture depends on the strength, concentration and spatial distribution of these obstacles and lies between a simple linear addition and the Pythagorean superposition [6]. The first approximation is expected for the superposition of very few strong obstacles among many weak obstacles. Such a case could correspond to the ferritic model alloys which only have few particles in the initial state. Especially for the case of a high particle strengthening effect in the initial state like the VVER 440-type RPV steel, the square-root superposition is the better approximation. Thus, one should strictly make a distinction between the effective radiation hardening as measured ($= \Delta R_{p0.2}$) and the 'pure' strengthening effect due to the formation of radiation defects ($= \Delta\sigma_{\text{rad}}$).

Considering the Pythagorean superposition of the radiation effect $\Delta\sigma_{\text{rad}}$ and the particle strengthening $\Delta\sigma_{\text{part}}$ due to the primary particles on the one hand, and a linear superposition with the solid solution hardening on the other hand, the ratio between the radiation effect and the measured yield stress increase is

$$\frac{\Delta\sigma_{\text{rad}}}{\Delta R_{p0.2}} = \sqrt{\left(1+\frac{\Delta\sigma_{\text{ss}}^{*}}{\Delta R_{p0.2}}\right)^{2} + 2\frac{\Delta\sigma_{\text{part}}^{\text{un}}}{\Delta R_{p0.2}}\left(1+\frac{\Delta\sigma_{\text{ss}}^{*}}{\Delta R_{p0.2}}\right)}, \quad (5)$$

with

$$\Delta\sigma_{\text{ss}}^{*} = \Delta\sigma_{\text{ss}}^{\text{un}} - \Delta\sigma_{\text{ss}}^{\text{irr}}.$$

or, when the strengthening phenomena are related to the yield stress $R_{p0.2}^{\text{un}}$ in the as-received condition

$$\frac{\Delta\sigma_{\text{rad}}}{\Delta R_{p0.2}} = \sqrt{(1+\eta/\kappa)^{2} + 2\lambda/\kappa(1+\eta/\kappa)} \quad (6)$$

with

$$\eta = \frac{\Delta\sigma_{\text{ss}}^{*}}{R_{p0.2}^{\text{un}}}, \quad \kappa = \frac{\Delta R_{p0.2}}{R_{p0.2}}, \quad \lambda = \frac{\Delta\sigma_{\text{part}}^{\text{un}}}{R_{p0.2}^{\text{un}}}.$$

In Fig. 7, the ratio $\Delta\sigma_{\text{rad}}/\Delta R_{p0.2}$ is depicted in dependence on the relative particle strengthening in the unirradiated condition (λ) and the relative radiation hardening measured (κ) for the cause that the solid solution strengthening is negligible ($\eta = 0$) or of relevance ($\eta = 0.2$). On the one hand, the effective radiation hardening $\Delta R_{p0.2}$ does only represent the pure radiation defect contribution $\Delta\sigma_{\text{rad}}$ if

$$\frac{\Delta\sigma_{\text{rad}}}{\Delta R_{p0.2}} \approx 1.$$

Fig. 7 clearly shows that the ratio is only approximately equal to 1 for a high effective radiation effect (that is

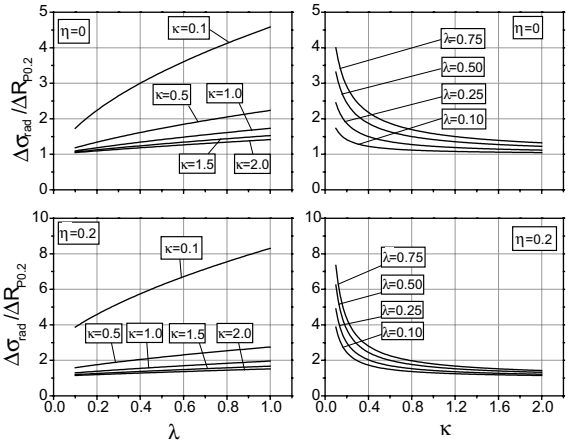

Fig. 7. Ratio between the irradiation strengthening $\Delta\sigma_{\text{rad}}$ and the increase of the yield stress after irradiation $\Delta R_{p0.2}$ as function of the normalized contribution of particle strengthening λ and the relative effective irradiation hardening κ.

irradiation up to high fluence) and especially for a low particle strengthening contribution in the as-received condition. On the other hand, Fig. 7 also demonstrates that close correlations between the radiation hardening and the volume fraction of the radiation defects cannot be expected when steels with different initial microstructure and alloy composition are considered. The correlation fit found, thus, is only a rough estimation valid for VVER-type base metal and ASTM RPV steels. A detailed analysis needs far more experimental efforts and better designed irradiation experiments.

Radiation embrittlement manifested by the shift of the transition temperature is usually combined with radiation hardening. One of the first developed models of neutron embrittlement uses a linear correlation between transition temperature shift and the yield stress increase [10]. The approximation is based on the model that the cleavage fracture in the lower shelf range is stress-controlled and occurs when the maximum tensile stress ahead the crack or notch tip exceeds a critical value $\sigma_{\text{f}}^{\text{eff}}$, which is defined as effective microscopic fracture stress [11,12]. The maximum tensile stress cannot become higher than a multiple of the yield stress. The level of the multiple is given by the plastic constraint. Whereas the fracture stress does not or hardly depend on the temperature, the yield stress of the ferritic steels exhibits a strong temperature dependence in the lower temperature range ($T <$ room temperature). In the frame of this simple model, the transition point is given by the temperature at which the multiple of the yield stress reaches the fracture stress $\sigma_{\text{f}}^{\text{eff}}$.

According to Dahl [13] the temperature dependence of the thermally activated dislocation movement follows an Arrhenius equation. Under consideration of an

athermal flow stress contribution σ_i, the yield stress obeys the equation

$$R_{p0.2} = \sigma_i + \sigma_0^* \left[1 - \frac{kT \ln \dot{\varepsilon}_0/\dot{\varepsilon}}{\Delta G^0}\right]^m. \quad (7)$$

The quantity σ_0^* is the thermal flow stress at $T = 0$ K, ΔG^0 is the free energy of activation enthalpy for overcoming the dislocation barrier necessary at zero effective stress, $\dot{\varepsilon}_0$ is the material-dependent strain rate constant, $\dot{\varepsilon}$ is the strain rate, m is a material constant and kT are the symbols as usual.

With $\sigma_f^{\text{eff}} = \alpha R_{p0.2}$ and under the assumption that the constants $\Delta G^0, \dot{\varepsilon}_0$, m, σ_f^{eff} and the thermally activated flow stress contribution are not affected by irradiation, the ductile to brittle transition temperature TT is given by

$$\text{TT} = \left[1 - \left(\frac{\frac{\sigma_f^{\text{eff}}}{\alpha} - \sigma_i}{\sigma_0^*}\right)^{1/m}\right] \frac{\Delta G^0}{k \ln \dot{\varepsilon}_0/\dot{\varepsilon}}, \quad (8)$$

$$\text{TT}_{\text{irr}} - \text{TT}_{\text{un}} = \frac{\Delta G^0}{\sigma_0^{*1/m} k \ln \dot{\varepsilon}_0/\dot{\varepsilon}} \times \left[\left(\frac{\sigma_f^{\text{eff}}}{\alpha} - \sigma_{i_{\text{irr}}}\right)^{1/m} - \left(\frac{\sigma_f^{\text{eff}}}{\alpha} - \sigma_{i_{\text{un}}}\right)^{1/m}\right]. \quad (9)$$

The model strictly simplifies the real condition but seems to be applicable as long as the mode of the fracture is changed. The experiments show no evidence for change of the fracture mode.

Thus, ΔTT is approximately proportional to $\Delta R_{p0.2}$ under the assumption that (a) $R_{p0.2}$ is measured at room temperature (low thermally activated contribution) and (b) the transition temperature is not too high ($\text{TT}_{\text{irr}} < 0$ °C). The proportionality factor, however, depends clearly on the material composition and condition. The relation between ΔTT and $\Delta R_{p0.2}$ data is illustrated in Fig. 8. The data show significant scattering but the trend for a group of different RPV steel types is convincing and is given by the relationship

$$\Delta\text{TT}/K = 0.6139 \Delta R_{p0.2}/\text{MPa} \pm 39.7, \quad R = 0.866. \quad (10)$$

A lack of agreement is again found for the model alloys and for the heat AR-W from the highly irradiated and embrittled VVER-440 weld material.

A square-root dependence of the transition temperature shift on the volume fraction of the radiation defects can be derived from the relationships (2) and (10). This relation is shown in Fig. 9. There are again a general correlation trend but also considerable deviations. A linear regression analysis of the data yields the least squares fit equation

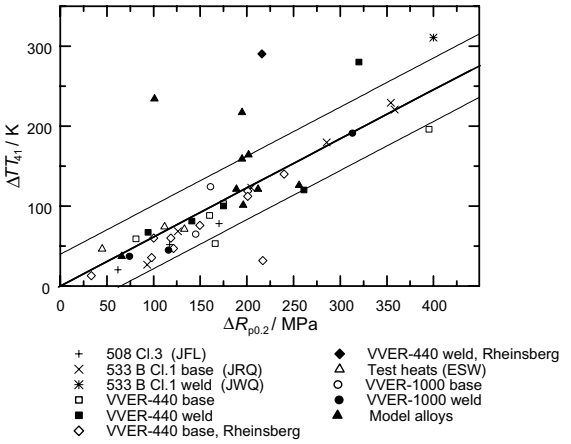

Fig. 8. Correlation between the shift of transition temperature ΔTT_{48} and the yield stress increase $\Delta R_{p0.2}$.

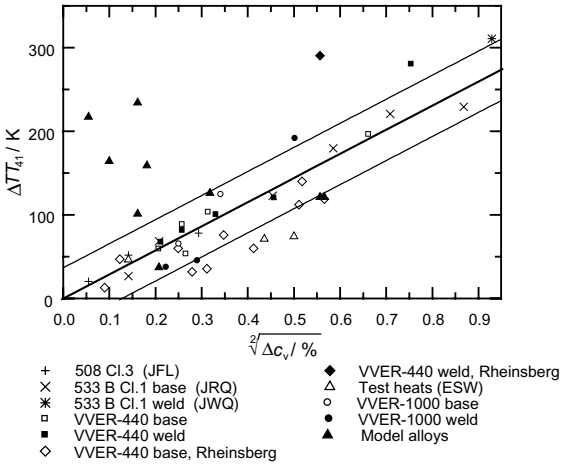

Fig. 9. Correlation between the shift of the transition temperature ΔTT_{48} and the square root of the volume fraction Δc_v of the irradiation defects.

$$\Delta\text{TT}/K = 288.2 \cdot \sqrt{\Delta c_v/\%} \pm 36.7 \quad (11)$$

with the correlation coefficient $R = 0.887$. The model alloys partly show a very high shift of the transition temperature, these results were not included in the regression analysis. Clearly, higher ΔTT-values are also measured for the VVER-440 weld metals whereas the VVER-440 base metals preferentially are below the correlation line. The ASTM RDB steels are well described by Eq. (11). Evidently, the efficiency of the radiation defects regarding the shift of the transition temperature differs for the different material types. The high sensitivity of the VVER-440 weld metals cannot be explained by the change of the fracture mode because the experimental findings do not indicate the presence of extraordinary phenomena.

6. Conclusions

A series of commercial RPV steels and model alloys were irradiated to fluences between 2.5 and 630×10^{18}/cm^2 [$E > 0.5$ MeV] in a neutron spectrum and under thermal conditions representative for VVER reactors. The bainitic VVER-type and ASTM-related RPV steels and the ferritic Fe-base model alloys exhibit nano-scaled microstructural features which can definitely be detected by SANS. Types and compositions of the materials as well as the neutron fluences hardly affect the characteristics of the features but change the volume fraction of the defects. There is a clear trend, the bigger the volume fraction, the higher the irradiation-induced increase of hardness and strength and the larger the shift of the transition temperature. The correlations approximately follow a square-root dependence. However, the proportionality is also influenced by the type of material and, thus, it is not possible to predict the changes in strength or toughness on the base of microstructural analyses using a generally valid correlation. The neutron embrittlement as identified by the transition temperature shift is a consequence solely of the irradiation hardening. In the first approximation there is no evidence that additional microstructural phenomena which are not detectable by SANS are of essential influence on the mechanical properties of the material investigated.

Acknowledgements

The authors acknowledge the many colleagues who have contributed to this work including the colleagues from RRC Kurchatov Institute Moscow and Paks NPP (Hungary), especially Messrs Ya.I. Strombakh, and A. Kruykov for the delivery of materials and data, as well as Mrs M.-H. Mathon from LLB Saclay, Mr P. Strunz from HMI Berlin and Mr C. Dewhurst from ILL Grenoble for supporting SANS measurements and for helpful discussions of the results. The work is based on results obtained in the frame of projects sponsored by the Bundesministerium für Wirtschaft und Technologie (GRS 150 0919, 150 10120).

References

[1] J. Böhmert, M. Große, A. Ulbricht, Nachweis, Interpretation und Bewertung neutroneninduzierter Defektstrukturen bei WWER-Reaktor-Druckbehälterstählen, Forschungszentrum Rossendorf, Wissenschaftlich-technische Berichte, FZR-381, 2003.
[2] O. Glatter, J. Appl. Crystallogr. 13 (1980) 7.
[3] M. Große, J. Böhmert, R. Gilles, J. Nucl. Mater. 254 (1998) 143.
[4] M. Große, V. Denner, J. Böhmert, M.-H. Mathon, J. Nucl. Mater. 277 (2000) 280.
[5] A. Ulbricht, J. Böhmert, P. Strunz, C. Dewhurst, M.-H. Mathon, Appl. Phys. A 74 (Suppl.) (2002) 1128.
[6] B. Reppich, Particle Strengthening, in: R.W. Cahn, P. Haase, E.J. Kramer (Eds.), Materials Science and Technology – A Comprehensive Treatment, in: H. Mugrabi (Ed.), Plastic Deformation and Fracture of Materials, vol. 6, Weinheim, 1993, p. 316.
[7] K.C. Russell, L.W. Brown, Acta Met. 20 (1972) 969.
[8] R.B. Schwarz, R. Labusch, J. Appl. Phys. 49 (1978) 1129.
[9] J.W. Martin, Micromechanisms in Particle-Hardened Alloys, Cambridge, 1980.
[10] S.B. Fisher, J.T. Buswell, J. Press. Vess. Piping 27 (1987) 91.
[11] R.O. Ritchie, J.F. Knott, J.R. Rich, J. Mech. Phys. Solids 21 (1973) 395.
[12] W. Dahl, Stahl und Eisen 101 (1981) 967.
[13] W. Dahl, Mechanische Eigenschaften, in: Werkstoffkunde Stahl, Bd. 1, Grundlagen, Berlin, 1984, p. 257.